International Journal of Mass Spectrometry 281 (2009) 150–156

Contents lists available at ScienceDirect

International Journal of Mass Spectrometry

journal homepage: www.elsevier.com/locate/ijms

Miniature ICR cells

F. Luebkemann*, K.P. Wanczek

University of Bremen, Institute of Inorganic and Physical Chemistry, NW2/Leobener Str., 28359 Bremen, Germany

ARTICLE INFO

Article history:
Received 22 September 2008
Received in revised form 28 January 2009
Accepted 28 January 2009
Available online 6 February 2009

Keywords:
SIMION
FT-ICR
Miniaturization

ABSTRACT

ICR cells with 2 and 4 mm radius have been characterized. In addition the trapping potential of the 4 mm cells was modified with wire mesh screening electrodes to yield a "particle in a box" potential. It was shown that ions of low m/z can be trapped. The performance of the cells varies with parameter changes especially at 2 mm cell radius. Peak splitting and mass shifts were observed in spectra of SF_5^+. The results from the 4 mm cells were comparable to those from larger cells with $r = 21$ mm. Potentials and ion trajectories were simulated with SIMION. The effective cyclotron frequency ω_+ was calculated by Fourier transformation of simulated transients and shown to depend on the ion's axial coordinate.

1. Introduction

The aim of this study is to investigate the effect of reduced size on performance of an ICR cell, on dynamic range, mass precision and resolution. Also it would be interesting to find out if there is a limit to miniaturization.

In an ICR cell ions are confined in the x–y plane by a magnetic field which induces the cyclotron motion and axially, along the magnetic field lines, by a static electric field. Paul traps on the other hand use time varying electric fields to trap ions.

The mass to charge ratio of the ions in an ICR cell is deduced from its cyclotron frequency via image charge detection. Various geometries have been developed to improve excitation/detection and trapping fields, e.g., open and closed cells of cubic and cylindrical shape [1]. Numerous efforts have been made to modify the potential inside these cells with additional electrodes. Segmented trapping electrodes, e.g., lead to a linear excitation potential for reduced z-excitation [2,3]. A central electron beam during the detection period stabilizes the ion cloud and leads to a longer transient [4]. Screened cells have been built for elimination of trapping potential inside the cell to reduce magnetron motion [5].

Penning-traps with electrodes of exact hyperboloidal shape exhibit an exact quadrupolar trapping field that is ideal for ion storage but produce a poor excitation field. Another approach is the "linearization" [6] of an ICR cell that minimizes higher order terms of the trapping potential by choosing a suitable aspect ratio. A number of miniature Penning-traps have been employed in physics for precision measurements and particle storage [7,8]. Also planar traps [9] have been realized in sub-mm size for electron storage. However, only very little literature exists on miniature ICR instruments and cells for analytical and field applications. The mobile ICR mass spectrometer "Quantra" manufactured by Siemens AG has an ICR cell with distinctly smaller dimensions than usual. For space flight, a miniature ICR instrument with a permanent magnet has been designed [10]. A transportable permanent magnet ICR instrument "Micra" has also been developed by Mauclaire et al. [11]. Its portability permits coupling to additional external spectrometers (e.g., a Free Electron Laser) for the analysis of intermediates in chemical reactions.

In contrast to this, miniature Paul traps are already well described and have also been realized on a mm scale both in single trap and array format [12–15]. Sector field instruments have been miniaturized as well [16].

The miniaturization of an ICR mass spectrometer with a miniature ICR cell has much promise for mobile mass spectrometers. Very small ICR cells might be employed in ICR instruments with high field superconducting magnets with a small room temperature bore for special applications in ultrahigh resolution analytical mass spectrometry. A number of important performance parameters depend on magnetic field strength [17]. For those that are especially relevant to small cells, like upper mass limit, maximum ion trapping time and onset of peak coalescence it would be advantageous to use the strongest available magnet, especially for high mass ions. Very high magnetic field strengths are offered by NMR magnets whose standard room temperature bore of usually 54 mm is too small for conventional ICR cells however. Miniaturized cells might offer access to magnets with small room temperature bores. For practical applications cells with radii smaller than 1 cm seem technically feasible. Use of these magnets would require a layout of the vacuum system for a vertical magnet bore. This has already been

* Corresponding author.
E-mail address: frank.luebkemann@gmx.de (F. Luebkemann).

1387-3806/$ – see front matter © 2009 Elsevier B.V. All rights reserved.
doi:10.1016/j.ijms.2009.01.017

demonstrated including ion transfer to the ICR cell with a multipole ion guide [18,19]. In addition for these cells, the homogeneous region of the magnetic field can be smaller than for ICR cells of normal size.

Ion ejection occurs when the energy of the ions reaches a value where their cyclotron radii are approximately equal to the ICR cell radius. This limits the application of high excitation energies in ICR cells with small radii. However, if one wants to measure ion lifetimes by the ejection method, ICR cells with small radii are of advantage, because shorter ejection times can be reached and the detection of metastable ions with short lifetimes becomes possible [20]. This method is based on an adaptation of the MIKES technique to ICR mass spectrometry by Anicich et al. [21], McMahon and Audier [22] and Freiser and coworkers [23]. In this technique a selected metastable ion is continuously ejected during the reaction time. A metastable ion with a lifetime longer than the ejection time does not dissociate before it has been removed from the cell and therefore its product ions ideally do not appear in the mass spectrum.

Rappmund [20] has found a minimum lifetime of 12.3 μs for the proton-bridged heterodimer of pyridine and dimethylamine with an excitation voltage of 150 V_{p-p} in a cell with 7 mm radius. This is about one order of magnitude less than ejection times reported by Freiser and coworkers [23] for a cell with 1 in. radius. Ion lifetimes of this magnitude can normally only be examined in sector field instruments.

Also a greater sensitivity has been found for miniaturized ICR cells. The smaller detection electrodes lead to a lower capacity of the detection circuit. Theoretically with the calculated signal voltages derived from the rotating monopole signal model [24] the detection of single charges should be possible with a signal to noise ratio of 1 [20]. This is in itself not a new feature for Penning-traps and has been demonstrated for multiply and singly charged single ions [25,26] but normally requires cryogenic cooling of the detector circuit and trap.

This is the first published report of the application of miniaturized ICR cells to the examination of ion/molecule reactions.

2. Theory

The electrostatic trapping potential $\Phi_T(r,z)$ in the center of an ICR cell can be expressed as [27]:

$$\phi_T(r,z) = V_T\left(\gamma - \frac{\alpha}{2d_0^2}(r^2 - 2z^2)\right) \quad (1)$$

where V_T is the trapping voltage, α and γ are constants depending on cell dimensions and d_0 is the characteristic cell dimension. In this ideal quadrupolar potential higher order terms of the trapping potential are neglected.

The motion in the *xy*-plane can now be described as a superposition of a fast *effective cyclotron motion* with a frequency ω_+ and a slow drift-like *magnetron motion* with a frequency ω_-. The difference between the unperturbed cyclotron frequency ω_c and ω_+ is largely governed by the axial frequency ω_z. This in turn depends on a number of experimental and cell-parameters. For an ion of mass m and charge q the axial frequency ω_z is:

$$\omega_z = \left(\frac{2qV_T\alpha}{md_0^2}\right)^{1/2} \quad (2)$$

$$\omega_\pm = \frac{\omega_c}{2} \pm \sqrt{\left(\frac{\omega_c}{2}\right)^2 - \frac{\omega_z^2}{2}} \quad (3)$$

For a given trap size ω_z increases proportionally to the trapping voltage and to $1/m$. This means that the difference between ω_c and ω_+ becomes large at high trapping voltage and high mass. Furthermore, for $\omega_z^2/2 > (\omega_c/2)^2$ the radicand in (3) becomes negative. In this case the ion motion is no longer stable and the ion is lost from the trap. As ω_z grows with $1/d^2$ this effect is especially important in very small cells. Lower trapping voltages diminish this effect.

Table 1
The critical parameter π_{trap} for m/z = 10, 100 and 1000 at 3 V trapping potential and a magnetic field strength of 7.05 T.

Cell radius (mm)	π_{trap}		
	m/z = 10	m/z = 100	m/z = 1000
0.5	0.050776	0.507759	5.077592
1.0	0.012694	0.126940	1.269398
2.0	0.003173	0.031735	0.317350
3.0	0.001410	0.014104	0.141044
4.0	0.000793	0.007934	0.079337
5.0	0.000508	0.005078	0.050776
6.0	0.000353	0.003526	0.035261
7.0	0.000259	0.002591	0.025906
8.0	0.000198	0.001983	0.019834
9.0	0.000157	0.001567	0.015672
10.0	0.000127	0.001269	0.012694
50.0	0.000005	0.000051	0.000508
100.0	0.000001	0.000013	0.000127

From the above equations one can derive a trapping potential dependent upper mass limit:

$$\left(\frac{m}{z}\right)_{critical} = \frac{B_0^2 d_0^2}{4V_T\alpha} \quad (4)$$

A new critical parameter π_{trap} was formulated by Schweikhard et al. [28]:

$$\pi_{trap} = 2\frac{\omega_z^2}{\omega_c^2} \quad (5)$$

For values of π_{trap} between 0 and 1 ion motion is stable in a quadrupolar potential. Table 1 shows the evolution of π_{trap} with cell radius for m/z ranging from 10 to 1000.

A plot of the frequencies of motion in a quadrupolar field also shows that at a trapping voltage of V_T = 3 V an ion of m/z = 1000 should still be trapped in a cell with 2 mm radius (Fig. 1). At a cell radius of 1 mm the ion motion is already unstable. Therefore the cells used in this study should be able to trap small molecules without problems.

The cross terms in a real trapping potential lead to coupling of axial and radial modes of motion [29]. A solution to this problem should be a pure quadrupolar potential [6] or a "particle in a box"

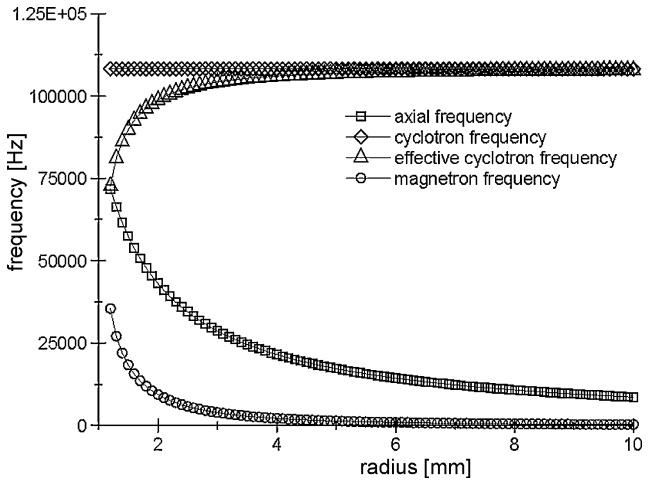

Fig. 1. Calculated frequencies of motion in Hz for an ion of m/z = 1000 at 3 V trapping potential and a magnetic field strength of 7.05 T.

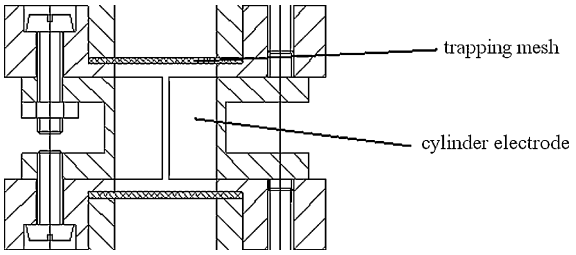

Fig. 2. Cutaway drawing of the miniaturized ICR cells without screening electrodes. Radii of the cylinder electrodes were $r = 2$ mm or 4 mm. The segmented cylinder electrodes include the structures for assembling the cell.

potential in which the ions experience no axial field between the screening electrodes. Ion-ion interactions are not included in this approach. Strictly this describes only single ion motion.

3. Methods

3.1. Instrumentation

The mass spectra were acquired with a modified prototype Bruker CMS47X FTICR spectrometer with a 7.05 T superconducting magnet with an 89 mm room temperature bore, described previously [30]. The standard vacuum system was evacuated with an oil diffusion pump (Varian VHS 600) with a liquid nitrogen cooled cryo-baffle and additional forepump (Edwards RV12). The pressure in the inlet system was 2×10^{-2} mbar. In the UHV system a base pressure of 1×10^{-8} mbar was reached. The pressure was measured with a Bayard-Alpert type hot-cathode gauge (Varian UHV-24p), in the inlet system with a Pirani gauge.

For this study cylindrical ICR cells with a radius of 2 mm with aspect ratio of 1 and of 4 mm radius with several aspect ratios mentioned below and segmented detection and excitation electrodes were used (Fig. 2). These were compared to the standard ICR cells with radius $r = 20$ mm and an aspect ratio of 1. The cylinder electrodes were made of non-magnetic stainless steel, trapping electrodes were made from platinum wire mesh with a wire spacing of 0.5 mm and a wire diameter of 0.1 mm. VESPEL was used as insulator material. An externally mounted rhenium filament served as cathode.

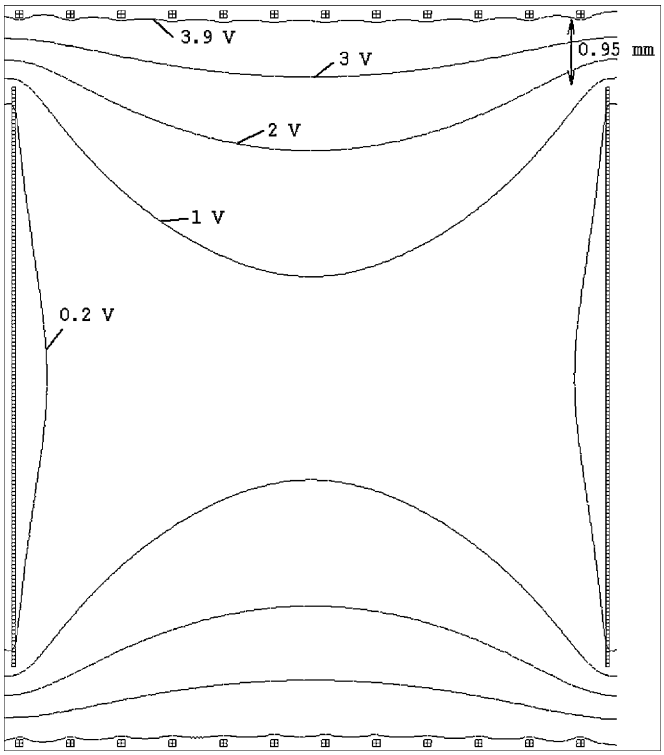

Fig. 3. Cross section of the 4 mm cell with equipotential lines. Trapping voltage was 4 V, the potential of the cylinder electrodes was 0.1 V.

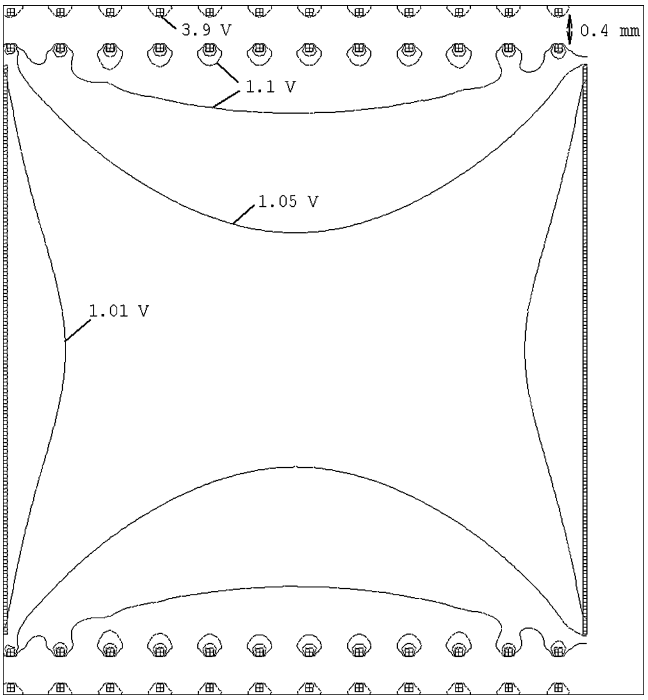

Fig. 4. Cross section of the 4 mm field corrected cell with equipotential lines. Trapping voltage was 4 V, the potential of the screening electrodes and the cylinder electrodes was 1 V.

Furthermore, ICR cells of 4 mm radius were employed with added screening electrodes in order to minimize the effects of the trapping potential. Three cylindrical ICR cells of 4 mm radius with wire mesh trapping and screening electrodes were used with aspect ratios of 0.5, 1 and 1.5. The trapping and screening electrodes were made from the same type of wire mesh. The potentials of the screening and trapping electrodes were regulated with two additional PC-mounted DAC-cards [31]. The distances between the electrodes are indicated in Figs. 3 and 4.

The cells were tested with SF_6 and Argon. Also the ion chemistry of the perfluoroalkyl silanes CF_3SiMe_3 and $C_2F_5SiMe_3$ was examined. Positive ions were generated by electron impact with an electron current of about 1 μA as measured with a Keithley Electrometer and an ionization time of 0.2 s. Electron energy usually was 70 eV. Negative ions were generated by dissociative electron attachment at 20 eV electron energy from the parent compounds. For excitation a chirp pulse was used with 2.2 μs pulse width per step and a step size of 10 kHz. The excitation voltage was typically 30 V_{P-P}. for the 2 mm cell and 90 V_{P-P}. for the 4 mm cell.

Figs. 3 and 4 show SIMION plots of the potential in the midplane of the cell including the positions of the trapping grids.

3.2. Computer-simulations

Ion trajectories and electric potentials inside the ICR cells were simulated with SIMION 7.0 for Windows [32]. This simulation program for charged particle optics calculates electrostatic fields in a user-defined configuration of electrodes. An iterative finite difference method is used for refining of the potential arrays. The

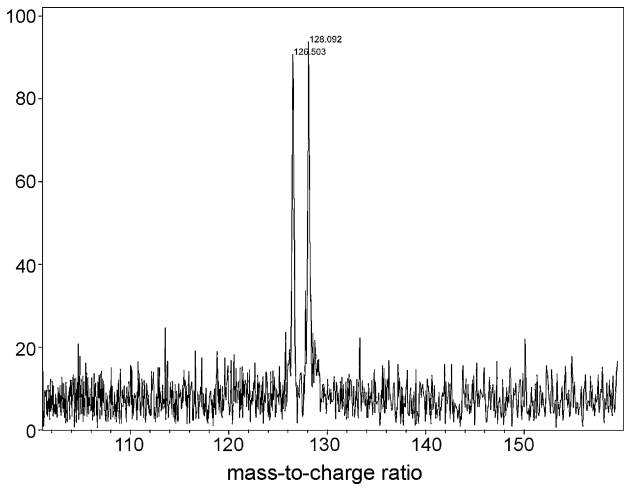

Fig. 5. Spectrum of SF_5^+ at $p = 4 \times 10^{-6}$ mbar pressure, cell radius 2 mm, $V_T = 3$ V, $m/\Delta m_{FWHM} = 511$ and 531.

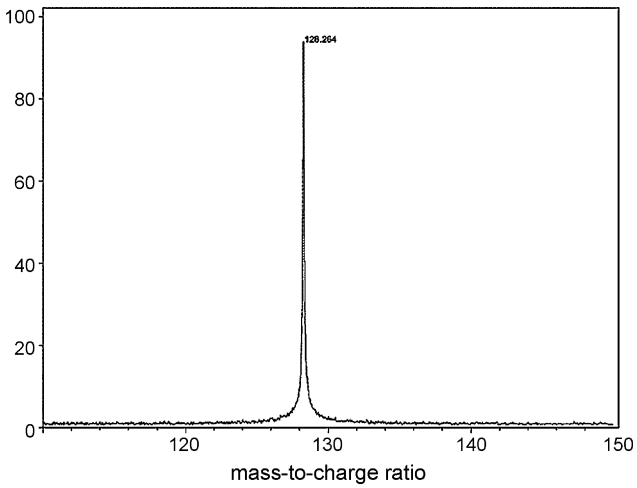

Fig. 6. Spectrum of SF_5^+ at $p = 2 \times 10^{-5}$ mbar pressure, cell radius 2 mm, $V_T = 3$ V, $m/\Delta m_{FWHM} = 1143$.

potential at each grid point is calculated from its next neighbours until a solution for the Laplace equation is found. The time steps for trajectory computation are determined with a fourth order Runge-Kutta integration method.

Space charge effects can at best be qualitatively demonstrated with SIMION (up to version 7). The treatment of ion-ion interactions would require a Poisson Solver as e.g., included in particle-in-cell method programs [33,34]. Therefore only single-ion trajectories were used in this study.

The trajectories were recorded with a modified version of the ICR user program included in the SIMION package that had been adapted to the geometries of the described cells. The spatial coordinates of the ion were recorded with SIMION at fixed time intervals as described in the SIMION "class" files (35) and exported to Diadem 10.2 (National Instruments). The time intervals were set to 0.5 μs to obtain a sampling frequency of 2 MHz. Fourier transformation yielded the frequency components of the simulated transient [35,36].

The frequencies of motion were also calculated with an Excel worksheet based on Eq. (3) and exported to Diadem for comparison. The appropriate cell constant α was calculated for the different aspect ratios [37].

Mechanical imperfections or misalignments generally were ignored in the simulations. A trial simulation with deliberately misaligned electrodes gave a deviation of 250 Hz for the effective cyclotron frequency of SF_5^+ in a cell with 2 mm radius. For this simulation a 2 mm cell was created with slightly tilted detection/excitation electrodes. Also one of the trapping grids was tilted 4° with respect to the z-axis and rotated 10° relative to the opposing trapping grid.

However, angular misalignment of the cell is predicted to promote damping of the cyclotron motion [6]. As the damping term γ is calculated to be proportional to $1/r^4$ this could be especially relevant for small traps.

4. Results and discussion

4.1. Spectra

4.1.1. 2 mm cell

For the first time spectra have been recorded with a 2 mm radius ICR cell. The excitation voltage had to be kept low enough to prevent radial ion ejection (≈30 V_{p-p}).

In contrast to normal behavior of ICR cells the smallest (2 mm) cell yields better spectra at higher pressures. At low pressures considerable peak splitting and sidebands were observed. The measured frequencies are sometimes higher than the unperturbed cyclotron frequency. This cannot be explained with trapping field or space charge effects as these lower the frequency. Also a mass shift of about 1 Da was observed for SF_5^+. The experiments showed that a trapping voltage of ≥3 V is necessary for the acquisition of spectra. Also a short time delay of 0.01 s before the excitation usually improved the signal. These observations may be due to collisional cooling of the ions.

In general, the operational behavior of the 2 mm cell is more unstable compared to normal ICR cells, leading to less reproducible results. At these small sizes the electric field gradients become very steep and the part of the potential where the influence of the trapping grids is effective is much larger compared to normal cells so that ions formed at the center of the cell or near the trapping nets experience very different potentials which probably leads to the marked peak splitting (Fig. 5). The same applies to the nonlinear part of the excitation potential at the edges of the excitation electrodes that may lead to z-ejection of ions.

At the even higher pressure of 2×10^{-5} mbar only one signal remains which exhibits a pronounced mass shift (Fig. 6) towards higher m/z.

In these small cells an increased amount of space-charge effects and therefore a broadening of the peaks can be expected. Although the number of ions that are created by electron ionization depends on the cell length the smaller accessible cyclotron radii and the low amplitude of the trapping motion will lead to a strong ion–ion interaction. This corresponds to an additional component of the trapping potential that results in a lowering of the effective cyclotron frequency [38]. In addition at high ion densities "phase-locking" phenomena [39] are observed which means that closely spaced peaks in the mass spectrum are no longer resolved.

The number of ions created during the ionization time can be estimated [40] as:

$$N_I = \frac{1}{e} T_I I_e l_e p S_e \quad (6)$$

e is the elemental charge, T_I is the ionization time, I_e is the ionization current in mA, l_e is the length of the cell, p is the pressure in mbar, S_e is the ionization coefficient. For this estimation the S_e for N_2 at 100 eV ionization energy was used [41].

In order to keep the number of ions low the ionization time P2 was reduced to 0.01 s in the 2 mm cell. At $p = 4 \times 10^{-6}$ mbar (Fig. 5) this gives an estimated number of 750 ions and 3.75×10^3 ions at $p = 2 \times 10^{-5}$ mbar (Fig. 6).

The maximum number of ions that still allows two peaks that are spaced Δm apart to be resolved can be estimated according to Mitchell and Smith [42] as follows:

$$N_{max} \approx 1.1 \times 10^{11} \left[\frac{B_0^2 L R_c \rho_c \Delta m}{m^2} \right] \quad (7)$$

B_0 is the magnetic field strength, R_c is the cyclotron radius, ρ_c is the ion cloud radius, m is the ion mass, L is the length of the ion cloud.

Rearrangement of this formula to calculate Δm with $N_{max} = 750$ ions, shows that it should be possible to reach a space-charge limited $m/\Delta m \approx 35{,}000$ for SF_5^+ at $p = 4 \times 10^{-6}$ mbar. ρ_c was assumed to be 1 mm and R_c was derived from a SIMION simulation with the experimental detection parameters.

4.1.2. 4 mm cell

In this cell 750 ions are generated already at $p = 1 \times 10^{-7}$ mbar. With the same approach as for the 2 mm cell this should lead to a $m/\Delta m \approx 78{,}000$. The mass spectra recorded at $p = 1 \times 10^{-7}$ mbar however showed $m/\Delta m$ values of only 2000–4000. These are higher than those for the 2 mm cell which is predicted from Eqs. (6) and (7) and shows the effect of the greater cell volume for equal ion numbers. Yet in these broadband spectra space-charge effects cannot be the only limiting parameter. Broadband mass spectra recorded with a 21 mm cell at $p = 8 \times 10^{-8}$ mbar showed approximately the same $m/\Delta m$ values as the 4 mm cell although the above calculations would yield a $m/\Delta m \approx 9 \times 10^6$.

The ion chemistry of perfluoroalkylated silanes has been compared to results obtained previously with larger cells [43]. With the 4 mm cell the same fragments and products of ion/molecule reactions were observed at the pressures and reaction times applied in this study.

In the mass spectra of $(CH_3)_3SiCF_3$ and $(CH_3)_3SiC_2F_5$ the siliconium ions R_3Si^+ (R = CH_3 or F) were found as the major fragments. An F/CH_3 exchange via a rearrangement reaction of the molecular ion of $(CH_3)_3SiCF_3$ led to the formation of $(CH_3)_2FSi^+$. Clustering of fragment ions with neutral molecules led to formation of the fluoronium ion $[((CH_3)_3Si)_2F]^+$. Pentavalent siliconates could be prepared through dissociative electron attachment from $CF_3Si(CH_3)_3$.

No new fragments or adducts have been recorded with the miniaturized cells.

4.1.3. Field corrected cells

Spectra could be acquired with a particle-in-a-box trapping potential.

In a field corrected cell, the trapping potential is almost zero over the length of the ICR with a very steep increase close to the screening electrode. (A similar potential was produced by McIver in an elongated cubic cell with an aspect ratio of 4.75 [44]). With the cell of aspect ratio 1, trapping times are at least by a factor of 10 shorter than for our standard screened ICR with a radius of 21 mm and an aspect ratio of 1.

This is in accordance with the computer simulations of ions with starting points near the trapping electrodes. Ions created in the center of the cell remain trapped as in normal cells. Ions moving towards the screening electrodes however can be quenched at the screens whereas in cells without screening electrodes they are reflected (cf. SIMION simulations).

The shift of the measured cyclotron frequency is clearly measurable as predicted by theory. The unperturbed cyclotron frequency of SF_6^- is calculated as $\omega_c = 741593$ Hz. In the cell with 4 mm radius an ω_+ of 737,032 Hz was measured with a trapping potential of 4 V. In the field corrected cell with an aspect ratio of 1 an ω_+ of 740,448 Hz was measured with the trapping electrodes set to 4 V and screening and detection/excitation electrodes set to 1 V. This shows that the screening electrodes lower the potential inside the cell.

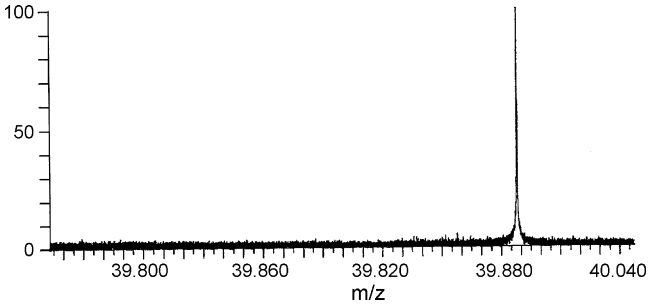

Fig. 7. High resolution spectrum of Ar^+ at a pressure of $p = 1 \times 10^{-7}$ mbar.

The same effect could be demonstrated in a field corrected cell of aspect ratio 1.5: with the trapping electrodes set to 4 V and screening and detection/excitation electrodes set to 1 V an ω_+ of 740,406 Hz was measured for SF_6^- at a pressure of 2×10^{-5} mbar. With the screening electrodes set to 4 V as well the frequency was shifted to 740,057 Hz. This shift towards deeper frequencies is expected as with this configuration there is now a normal trapping potential in the cell although its effect is slightly lowered by the increased aspect ratio of 1.5. At a pressure of 5×10^{-7} mbar with the trapping electrodes at 4 V, the screening electrodes set to 0.1 V and the detection/excitation electrodes set to 0 V an ω_+ of 741,200 Hz was measured. This is very close to the unperturbed cyclotron frequency and again demonstrates the effect of the particle-in-a-box trapping potential.

The best mass $m/\Delta m_{FWHM}$ obtained with the 4 mm field corrected cell was 120,000 for Ar^+ (Fig. 7) [45]. Neither experimentally nor in the computer simulations could any effect of the aspect ratio be observed.

Experiments with the elongated 4 mm cell showed that its performance is similar with screening electrodes at slightly higher potentials than the cylinder electrodes. This results in a still very shallow trapping potential with presumably less quenching of ions at the screening electrode wires.

4.2. Simion simulations

4.2.1. Potentials

The results of the SIMION calculations indicate that the potential in the miniaturized cells is a smaller version of the potential in conventional cells. However, the corresponding fields are much stronger.

With the results of Eqs. (1) and (2) the magnetron frequency ω_- can be expressed as:

$$\omega_- = \frac{\omega_c}{2} - \sqrt{\left(\frac{\omega_c}{2}\right)^2 - \frac{qE(r)}{mr}} \quad (8)$$

In this case $E(r)$ is the radial electric field $d\Phi_T/dr$. As the magnetron frequency is a function of $1/{d_0}^2$ through $E(r)$ the frequency shifts caused by deviations from the ideal quadrupolar trapping potential in small cells are very large.

For values of $\omega_c/2 \gg qE(r)/mr$ the root term can be approximated as:

$$\omega_- \approx \frac{\omega_c}{2} - \left(\frac{\omega_c}{2} - \frac{qE(r)}{mr\omega_c}\right) \quad (9)$$

If we insert $\omega_c = qB_0/m$ then ω_- becomes [46]:

$$\omega_- = \frac{E(r)}{rB_0} \quad (10)$$

With these approximations ω_- is not a function of m. The values of $E(r)$ at various z positions from the numerical solution of SIMION were used to calculate ω_- as a function of ion position. This

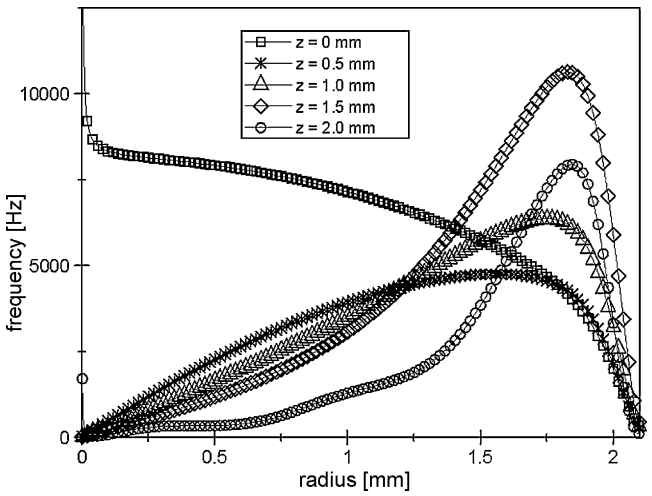

Fig. 8. Calculated ω_- as a function of $E(r)$ at different z positions at 3 V trapping potential.

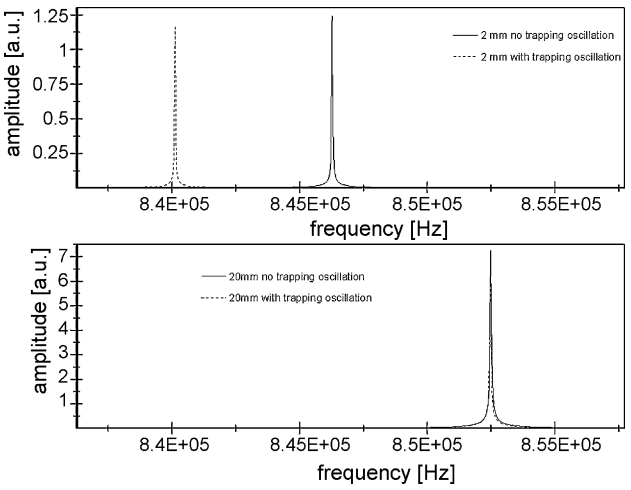

Fig. 9. Simulated ω_+ of SF_5^+ in cells with $r = 2$ and 20 mm with and without trapping oscillation. Ions were excited to ca. 75% of the maximum cyclotron radius.

approach strictly is valid only for the quadrupolar approximation of the trapping potential as only there axial and radial movements are decoupled.

Fig. 8 shows the magnetron frequencies calculated from Eq. (10) as a function of r at various z-positions in a 2 mm cell with the cell center defined as $z = 0$ mm.

The shape of $E(r)$ changes with axial position. In the center of the cell it is a saddle potential whereas near the trapping grids $E(r)$ increases towards the side electrodes. Different ω_- are expected for different ion positions.

SIMION was used to record the electric field and the ion's position with a test "ion" with no charge that flies unimpeded by fields.

4.2.1.1. Screened cell. SIMION simulations show that the screening electrodes at a potential of 0 V result in a strong reduction of the trapping potential. There is now approximately a particle-in-a-box potential in the cell (Fig. 4).

This should have the effect of a reduced magnetron motion and result in less peak splitting due to variations of the potential (cf. Frequencies section).

For a realistic simulation of ion motion in the vicinity of the grids it is vital that the wires are modeled as having a diameter of more than one grid unit. Otherwise they are treated as ideal electrodes by SIMION which means that they present no physical barrier for passage of the ions.

Although the shape of the potential inside the cell would still be correct, the wires of the screening electrodes constitute local potential wells because of the permeation of the trapping potential through the screen [45,47]. Therefore they should be modeled as having finite dimension i.e., with a diameter of at least 4 grid units. A simulation with non-ideal wires shows that ions that come to close collide with the wires and are neutralized. This is also observed during excitation where the axial component of the excitation field accelerates ions which are trapped at the edges of the cell in the direction of the trapping electrodes. Ions with large trapping amplitude can oscillate through the screens and can be neutralized when their cyclotron radius is increased.

SIMION trajectories also show that trapping electrodes made of wire mesh also induce a certain amount of cyclotron motion [48]. Deflection by the electric field from the wire causes a lateral ion movement perpendicular to magnetic field and thus cyclotron motion. This effect is different from ion reflection at ordinary trapping plates.

As a result it depends on the ion's position at the time of excitation whether it will remain in the cell or be quenched.

In screened cells the greater axial spread of the ion cloud should decrease the space-charge effects [45]. Also, because of the lower trapping potential ions of higher m/z can be trapped.

The Computer simulations indicate that the performance of the screened cells may depend on the grid constant of the screening electrodes. In our experiments, for the small cells the same mesh was used as for larger cells (cf. Instrumentation). A large distance between the wires permits a strong permeation of the trapping field through the screen which produces local potential minima at the screening electrode wires thus guiding the ions towards the electrode wires instead of repelling them.

A better approach would be to scale the grid constant proportionally to cell size. A denser mesh results in a more uniform potential barrier with improved field shape.

4.2.2. Frequencies

The frequencies ω_+ and ω_- can also be calculated from the simulated trajectories. With the SIMION data recording function the x-coordinate of the ions can be monitored and a following Fourier transformation of the simulated transient yields the frequencies ω_+ and ω_-.

The results show that in the small cells ions in the center of the cell move with distinctly different frequencies than ions with large trapping amplitude (Fig. 9). The quadrupolar approximation is obviously not valid, i.e., ω_+ and ω_- strongly depend on the ion's z-coordinate.

Fig. 9 shows the range of frequencies that occur due to different initial z-positions. In the large cell the peaks with and without trapping motion have only slightly different frequencies (7 Hz) and almost overlap.

The difference of ca. 60 kHz from the simulation of the 2 mm cell corresponds to $m/z \approx 0.9$ for the SF_5^+ signal calculated with Eq. (3). This does not completely explain the observed difference of 1.5 mass units in Fig. 3, however space-charge effects that further lower ω_+ have not been included in the simulations.

The simulated frequencies for a group of ions starting every 0.2 mm along the z-axis show a strong spreading of the frequency values (Fig. 10). In the simulation the ions were excited with the experimental parameters and then the trajectories were recorded. Fig. 10 shows that equal starting points result in equal frequencies. Ions created at the cell's center move with the highest ω_+. For the other ions no relation between starting point and simulated ω_+ can be found. The same applies for the varying peak heights. This clearly

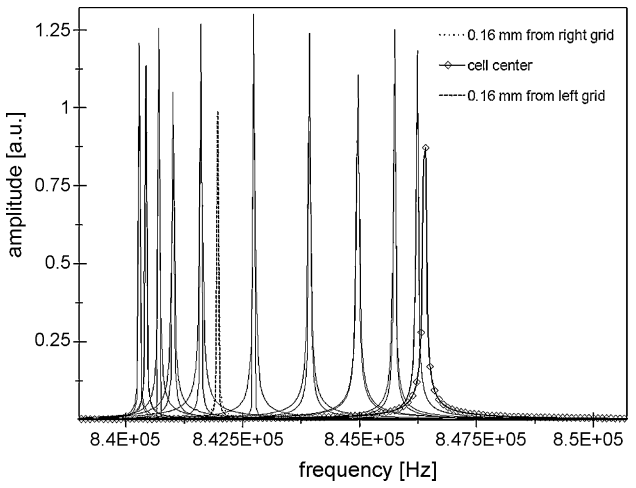

Fig. 10. Range of calculated ω_+ for ions with starting points spaced 0.2 mm apart. Selected ions are identified by their starting positions relative to the trapping grids.

indicates that the forces acting on the ions are not independent of the ion's coordinates along the z-axis and that the combined effect of nonlinear excitation potential and the nonquadrupolar trapping potential is not predictable.

Higher harmonics might also be expected as the ions come very close to the detection electrodes but have not been observed in the experiments.

5. Conclusion

In the smallest cell with $r = 2$ mm the measured cyclotron frequencies show strong deviations from values calculated by the methods applicable to cells of larger size. The quadrupolar approximation is no longer applicable.

Due to the decreased cell volume space-charge effects have a larger effect than in normal cells. The measured $m/\Delta m_{\mathrm{FWHM}}$ values are worse than predicted by space-charge limit. Another reason may be the trapping efficiency which is also expected to be lower because of the smaller radii:

$$t_{1/2} \propto \frac{d^2 B_0^2}{p V_{\mathrm{T}}} \tag{11}$$

$t_{1/2}$ is the time in which the ion concentration decreases to 50% of its initial value, d is the cell diameter [49].

A low trapping efficiency will lead to a short transient and so to a low $m/\Delta m_{\mathrm{FWHM}}$.

The spectra from cells with 4 mm radius show $m/\Delta m_{\mathrm{FWHM}}$ equal to those from cells of normal size.

A particle-in-a-box potential that diminishes the effects of the trapping potential inside the cell can be created in miniaturized cells through wire mesh screening electrodes.

The results indicate that applications in mobile spectrometers or the coupling with NMR magnets should be feasible with cells having radii $\geq$4 mm.

Acknowledgements

The authors thank the staff of the chemistry department's mechanical shop for building the ICR cells and their continuous support.

References

[1] S. Guan, A.G. Marshall, Int. J. Mass Spectrom. 146/147 (1995) 261.
[2] P. Caravatti, M. Allemann, Org. Mass Spectrom. 26 (1991) 514.
[3] S. Kim, M.C. Choi, M. Hur, H.S. Kim, J.S. Yoo, C.L. Hendrickson, A.G. Marshall Rapid Commun. Mass Spectrom. 22 (2008) 1423.
[4] N.K. Kaiser, C.R. Weisbrod, B.N. Webb, J.E. Bruce, J. Am. Soc. Mass Spectrom 19 (2008) 467.
[5] M. Wang, A.G. Marshall, Anal. Chem 61 (1989) 1288.
[6] S.E. Barlow, M.D. Tinkle, Rev. Sci. Instrum. 73 (2002) 4185.
[7] D.L. Donohue, L.D. Hulett Jr., S.A. McLuckey, G.L. Glish, H.S. McKown, Int. J. Mass Spectrom. Ion Processes 97 (1990) 227.
[8] G. Werth, Th. Beier, S. Djekic, H.-J. Kluge, W. Quint, T. Valenzuela, J. Verdu, M. Vogel, Nucl. Instr. Methods. Phys. Res. B 205 (2003) 1.
[9] S. Stahl, F. Galve, J. Alonso, S. Djekic, W. Quint, T. Valenzuela, J. Verdú, M. Vogel, G. Werth, Eur. Phys. J. D 32 (2005) 139.
[10] B. Wiezorek, Diploma Thesis, University of Bremen (1990).
[11] G. Mauclaire, J. Lemaire, P. Boissel, G. Bellec, M. Heninger, Eur. J. Mass Spectrom. 10 (2004) 155.
[12] H. Chen, R. Xu, H. Chen, R.G. Cooks, Z. Ouyang, J. Mass. Spectrom. 40 (2005) 1403.
[13] L. Gao, A. Sugiarto, J.D. Harper, R.G. Cooks, Z. Ouyang, Anal. Chem. 80 (2008) 7198.
[14] E.R. Badman, R.G. Cooks, Anal. Chem. 72 (2000) 3291.
[15] E.R. Badman, R.G. Cooks, Anal. Chem. 72 (2000) 5097.
[16] J.A. Diaz, C.F. Giese, W.R. Gentry, J. Am. Soc. Mass Spectrom. 12 (2001) 619.
[17] S. Guan, A.G. Marshall, Rapid Commun. Mass Spectrom. 10 (1996) 1819.
[18] C.L. Hendrickson, J.J. Drader, D.A. Laude Jr., S. Guan, Alan G. Marshall, Rapid Commun. Mass Spectrom. 10 (1996) 1829.
[19] C. Lin, R. Mathur, K. Aizikov, P.B. O'Connor, J. Am. Soc. Mass Spectrom. 18 (2007) 2090.
[20] A. Rappmund, PhD Thesis, University of Bremen (2000).
[21] V.G. Anicich, A.D. Sen, W.T. Huntress Jr., M.J. McEwan, J. Chem. Phys. 94 (1991) 4189.
[22] H.E. Audier, T.B. McMahon, J. Am. Chem. Soc. 116 (1994) 8294.
[23] C.-Y. Lin, Q. Chen, H. Chen, B.S. Freiser, J. Phys. Chem. A 101 (1997) 6023.
[24] M.B. Comisarow, J. Chem. Phys. 69 (1978) 4097.
[25] M. Diederich, H. Häffner, N. Hermanspahn, M. Immel, H.J. Kluge, R. Ley, R. Mann, W. Quint, S. Stahl, G. Werth, Hyperfine Interact. 115 (1998) 185.
[26] J. Ketelaer, Diploma Thesis, University of Mainz (2006) http://www.quantum.physik.uni-mainz.de/mats/publications/2006 Diplom Jens Ketelaer.pdf.
[27] M.A. May, P.B. Grosshans, A.G. Marshall, Int. J. Mass Spectrom. Ion Processes 120 (1992) 193.
[28] L. Schweikhard, J. Ziegler, H. Bopp, K. Lützenkirchen, Int. J. Mass Spectrom. 141 (1995) 77.
[29] P. Kofel, M. Allemann, Hp. Kellerhals, K.P. Wanczek, Int. J. Mass Spectrom. Ion Processes 74 (1986) 1.
[30] M. Allemann, Hp. Kellerhals, K.P. Wanczek, Chem. Phys. Lett. 75 (1980) 328.
[31] R. Malek, PhD Thesis, University of Bremen (1999) http://nbn-resolving.de/urn:nbn:de:gbv:46-diss000000411.
[32] D. Dahl, Int. J. Mass Spectrom. 200 (2000) 3.
[33] D.W. Mitchell, J. Am. Soc. Mass Spectrom. 10 (1999) 136.
[34] E.N. Nikolaev, R.M.A. Heeren, A.M. Popov, A.V. Pozdneev, K.S. Chingin, Rapid Commun. Mass Spectrom. 21 (2007) 3527.
[35] D.A. Dahl, A.D. Appelhans, ASMS Short Course 44th ASMS Conference, Portland, 1996.
[36] S.C. Beu, Proceedings of the 54th ASMS Conference, Seattle, 2006.
[37] G.S. Jackson, J.D. Canterbury, S. Guan, A.G. Marshall, J. Am. Soc. Mass Spectrom. 8 (1997) 283.
[38] T.J. Francl, M.G. Sherman, R.L. Hunter, M.J. Locke, W.D. Bowers, R.T. McIver Jr., Int. J. Mass Spectrom. Ion Processes 54 (1983) 189.
[39] A.J. Peurrung, R.T. Kouzes, Int. J. Mass Spectrom. Ion Processes 145 (1995) 139.
[40] P. Kofel, PhD Thesis, University of Bremen (1987).
[41] A.v. Engel, Ionized Gases, 2nd ed., Oxford University Press, 1965.
[42] D.W. Mitchell, R.D. Smith, Phys. Rev. E 52 (1995) 4366.
[43] F. Luebkemann, K.P. Wanczek, Int. J. Mass Spectrom. 278 (2008) 95.
[44] R.L. Hunter, M.G. Sherman, R.T. McIver Jr., Int. J. Mass Spectrom. Ion Phys 50 (1983) 259.
[45] F. Luebkemann, K.P. Wanczek, Proceedings of the 51st ASMS Conference, Montreal, 2003.
[46] S.E. Barlow, M.D. Tinkle, J. Appl. Phys. 99 (2006) 013306.
[47] D.A. Dahl, T.R. McJunkin, J.R. Scott, Int. J. Mass Spectrom. 266 (2007) 156.
[48] M. Bamberg, PhD Thesis, University of Bremen (1991).
[49] T.J. Francl, E.K. Fukuda, R.J. McIver Jr., Int. J. Mass Spectrom. Ion Phys 50 (1983) 151.